DOI 10.5162/Ultrasonic2025/P1.25

Change of Piezoelectric Signal Generated in Cancellous Bone by Ultrasound Irradiation Associated with Oblique Trabecular Orientation

Atsushi Hosokawa[1]
[1]National Institute of Technology, Akashi College, 679-3 Nishioka, Uozumi, Akashi, Japan,
hosokawa@akashi.ac.jp

Abstract: The piezoelectric signals generated in water-saturated cancellous bone with oblique trabecular orientations were numerically simulated. The waveforms of the piezoelectric signals in cancellous bone and the ultrasound signals through the bone when an ultrasound wave was irradiated were calculated. The simulated results suggested that the piezoelectric waves could primarily depend on the fast and slow waves in the ultrasound signals but could be also affected by the other factors.

Keywords: Cancellous bone, Piezoelectric signal, Trabecular orientation, Fast wave, Slow wave

Introduction

Bone is a piezoelectric material [1], and bone formation can be accompanied by the piezoelectric effects [2]. This mechanism is utilized in accelerating bone fracture healing using ultrasound [3]. To establish an ultrasound healing method for joint bones, it is essential to understand the piezoelectric properties in cancellous bone, which constitutes the majority of the epiphysis. As the ultrasound signals propagated through cancellous bone can change depending on the trabecular orientation [4], it is expected that the piezoelectric signals generated in the bone by ultrasound irradiation can be largely affected by the orientation. In the present study, the piezoelectric signals in water-saturated cancellous bone with oblique trabecular orientations were numerically simulated.

Methods

Numerical simulations of the piezoelectric signals in water-saturated cancellous bone were performed using a piezoelectric finite-difference time-domain (PE-FDTD) method, which is an advanced elastic FDTD method with piezoelectric constitutive equations. The governing equations are as follows [5].

$$\rho \frac{\partial v_i}{\partial t} = \frac{\partial \tau_{ii}}{\partial x_i} + \frac{\partial \tau_{ij}}{\partial x_j} + \frac{\partial \tau_{ik}}{\partial x_k} \tag{1}$$

$$\frac{\partial \tau_{ii}}{\partial t} = (\lambda + 2\mu)\frac{\partial v_i}{\partial x_i} + \lambda \frac{\partial v_j}{\partial x_j} + \lambda \frac{\partial v_k}{\partial x_k} - e_{ii}\frac{\partial E_i}{\partial t} - e_{ji}\frac{\partial E_j}{\partial t} - e_{ki}\frac{\partial E_k}{\partial t} \tag{2}$$

$$\frac{\partial \tau_{jk}}{\partial t} = \mu\left(\frac{\partial v_j}{\partial x_k} + \frac{\partial v_k}{\partial x_j}\right) - e_{il}\frac{\partial E_i}{\partial t} - e_{jl}\frac{\partial E_j}{\partial t} - e_{kl}\frac{\partial E_k}{\partial t} \tag{3}$$

$$\varepsilon_{ii}\frac{\partial E_i}{\partial t} = -e_{ii}\frac{\partial v_i}{\partial x_i} - e_{ij}\frac{\partial v_j}{\partial x_j} - e_{ik}\frac{\partial v_k}{\partial x_k} - \frac{e_{il}}{2}\left(\frac{\partial v_j}{\partial x_k} + \frac{\partial v_k}{\partial x_j}\right) - \frac{e_{im}}{2}\left(\frac{\partial v_k}{\partial x_i} + \frac{\partial v_i}{\partial x_k}\right) - \frac{e_{in}}{2}\left(\frac{\partial v_i}{\partial x_j} + \frac{\partial v_j}{\partial x_i}\right) + \frac{\partial D_i}{\partial t} \tag{4}$$

$$\frac{\partial D_i}{\partial t} = -\sigma_i E_i \tag{5}$$

In Eqs. (1)–(5), the variables are v_i of the particle velocity, τ_{ii} and τ_{ij} of the normal and shear stresses, E_i of the electric field, and D_i of the electric displacement. The constants are ρ of the density, λ and μ of the first and second Lamé coefficients, e_{ij} of the piezoelectric constant, ε_{ii} of the dielectric constant, and σ_i of the conductivity.

The simulation model is shown in Fig. 1. Three-dimensional (3D) X-ray microcomputed tomographic (μCT) images of cancellous bone were obtained from positions with porosities of 0.70 and 0.83 (70 and 83%) of a bovine femur. To create the 3D cancellous bone models with angles θ = 0–90 ° of the major trabecular orientation, each μCT image was rotated at θ, cut into a cube with a side length of 5.7 mm, and binarized into the values of the solid bone and the pore space. The pore spaces were saturated with water.

DOI 10.5162/Ultrasonic2025/P1.25

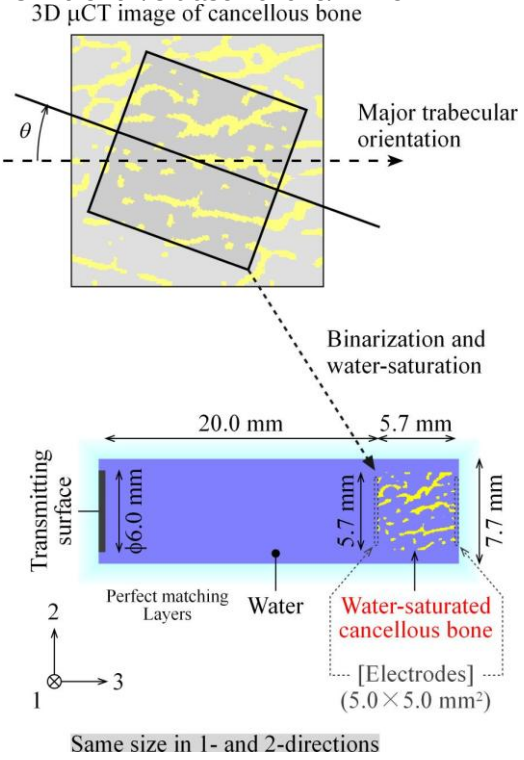

Fig. 1: Numerical model for simulating piezoelectric signals generated in cancellous bone with an oblique angle θ of the major trabecular orientation when an ultrasound wave is irradiated.

Tab. 1: Elastic [6,7] and piezoelectric [8–10] parameters in piezoelectric finite-different time-domain (PE-FDTD) simulations.

	Solid bone	Water
Density ρ (kg/m^3)	1960	1000
1st Lamé coefficient λ (GPa)	14.8	2.2
2nd Lamé coefficient μ (GPa)	8.3	0
Piezoelectric constants (μC/m^2)		
e_{31}, e_{32}, e_{33}	0.21	0
e_{14}, $-e_{25}$	1.32	0
e_{15}, e_{24}	0.26	0
Others	0	0
Dielectric constant ε (nF/m)	50.0	0.7

In the simulation model, the cancellous bone model was located at the position of 20 mm apart from the ultrasound transmitting surface with a diameter of 6.0 mm. The square electrodes with a side of 5.0 mm were assumed to be in the center of the front and back surfaces of the cancellous bone model. However, the electrodes were regarded as perfect conductors, and the elastic properties were ignored. Twenty grids of perfectly matched layers (PMLs) were set at all boundaries surrounding the simulation region. The spatial and temporal intervals were 57 μm and 3 ns, respectively. The elastic [6,7] and piezoelectric [8–10] constant values of the solid bone and water are listed in Tab. 1.

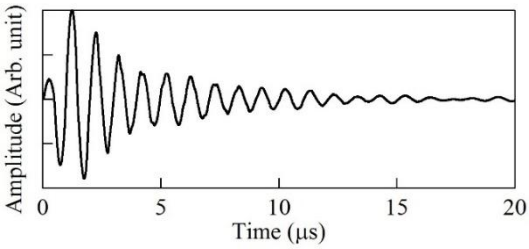

Fig. 2: An input waveform of ultrasound signal irradiated to cancellous bone in piezoelectric finite-difference time-domain (PE-FDTD) simulations.

The input of the irradiated ultrasound signal was the experimental signal emitted from a $Pb(Zr,Ti)O_3$ (PZT) ultrasound transmitter driven by one-cycle burst voltage at 1 MHz, and the waveform is shown in Fig. 2. The output was the piezoelectric signal generated in cancellous bone and the ultrasound signal propagated through the bone. The piezoelectric signal was calculated from the voltage (electric field) induced between the front and back electrodes, and the ultrasound signal was calculated from the normal stress on the surface of the back electrode.

Results and Discussion

The simulated waveforms for the cancellous bone models with porosities of 0.70 and 0.83 are shown in Figs. 3 and 4, respectively; (a) and (b) show the waveforms of the piezoelectric and ultrasound signals, respectively.

It is known that two ultrasound waves of “fast and slow waves” can propagate through water-saturated cancellous bone [11]. The fast and slow waves propagate mainly in the solid bone and the pore space parts, respectively. At the relatively low porosity, the fast wave amplitude becomes larger. Therefore, the fast wave was majorly observed at the porosity of 0.70 in Fig. 3(b). However, both the fast and slow waves were observed at the porosity of 0.83 in Fig. 4(b). Moreover, it is reported that the fast wave speed decreased with the ultrasound angle to the trabecular orientation [12]. Therefore, the first arrival time decreased with the angle θ of the major trabecular orientation. As a result, the overlap of the fast and slow waveforms became larger.

The piezoelectric signal waveforms in Figs. 3(b) and 4(b) were largely different from the ultrasound signal waveforms in Figs. 3(a) and 4(a). This was because the

DOI 10.5162/Ultrasonic2025/P1.25

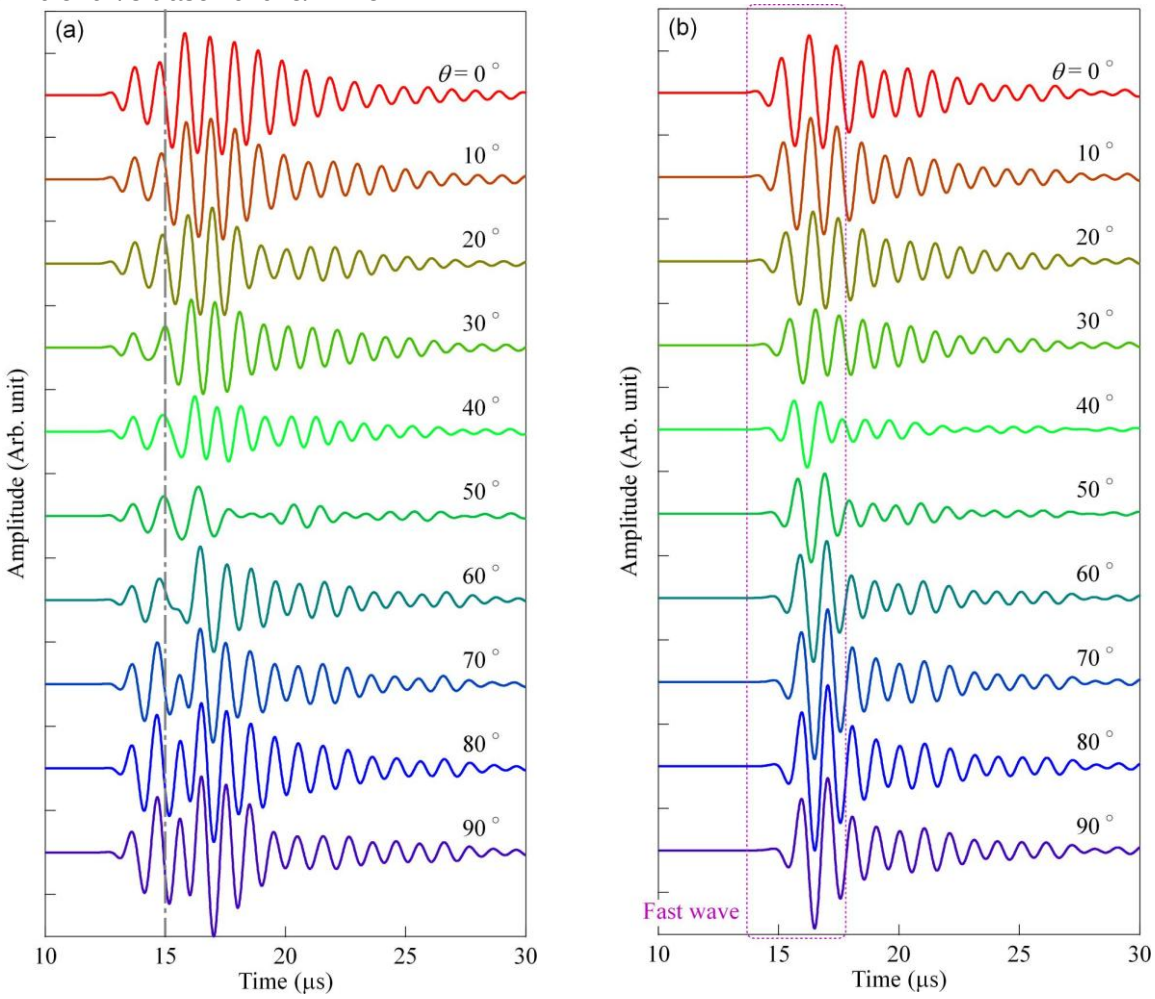

Fig. 3: Calculated waveforms for cancellous bones with a porosity of 0.70 and angles θ = 0–90 ° of the major trabecular orientation in piezoelectric finite-difference time-domain (PE-FDTD) simulations; (a) shows the piezoelectric signals generated in the bones, and (b) shows the ultrasound signals propagated through the bones.

piezoelectric signal detected between the electrodes or between the front and back surfaces of the cancellous bone specimen can be regarded as a superposition of piezoelectric signals generated at the local points in the ultrasound direction. Although it appeared that the piezoelectric signals could be separated into two waves, like the fast and slow waves in the ultrasound signal, the separation times in the signals at the porosities of 0.70 and 0.83 [Figs. 3(a) and 4(a)] were different, being about 15 and 17 μs, respectively. Moreover, the peak time of the wave after the separation time at the porosity of 0.70 increased with the angle θ of the major trabecular orientation, but the time at the porosity of 0.83 was almost constant. This was considered to be because the piezoelectric waves at the porosity of 0.70 could be majorly due to the fast wave, but the piezoelectric wave at the porosity of 0.83 could be majorly due to the slow wave. In the piezoelectric signals at the porosity of 0.83, the waves before 17 μs could be further separated, which was considered to be because the waves due to the fast and slow waves was mixed.

The changes in the piezoelectric signals did not necessarily agree with the changes in the ultrasound signals. The causes for this were considered to be the complex mixture of the piezoelectric waves due to the fast and slow waves, and the properties other than the ultrasound properties.

Conclusions

In the piezoelectric signals, two waves attributed to the fast and slow waves in the ultrasound signals were observed. The changes of the piezoelectric waves did not necessarily depend on only the changes of the fast and slow waves, which was suggested that the piezoelectric signals could be affected by factors other than the ultrasonic signals.

DOI 10.5162/Ultrasonic2025/P1.25

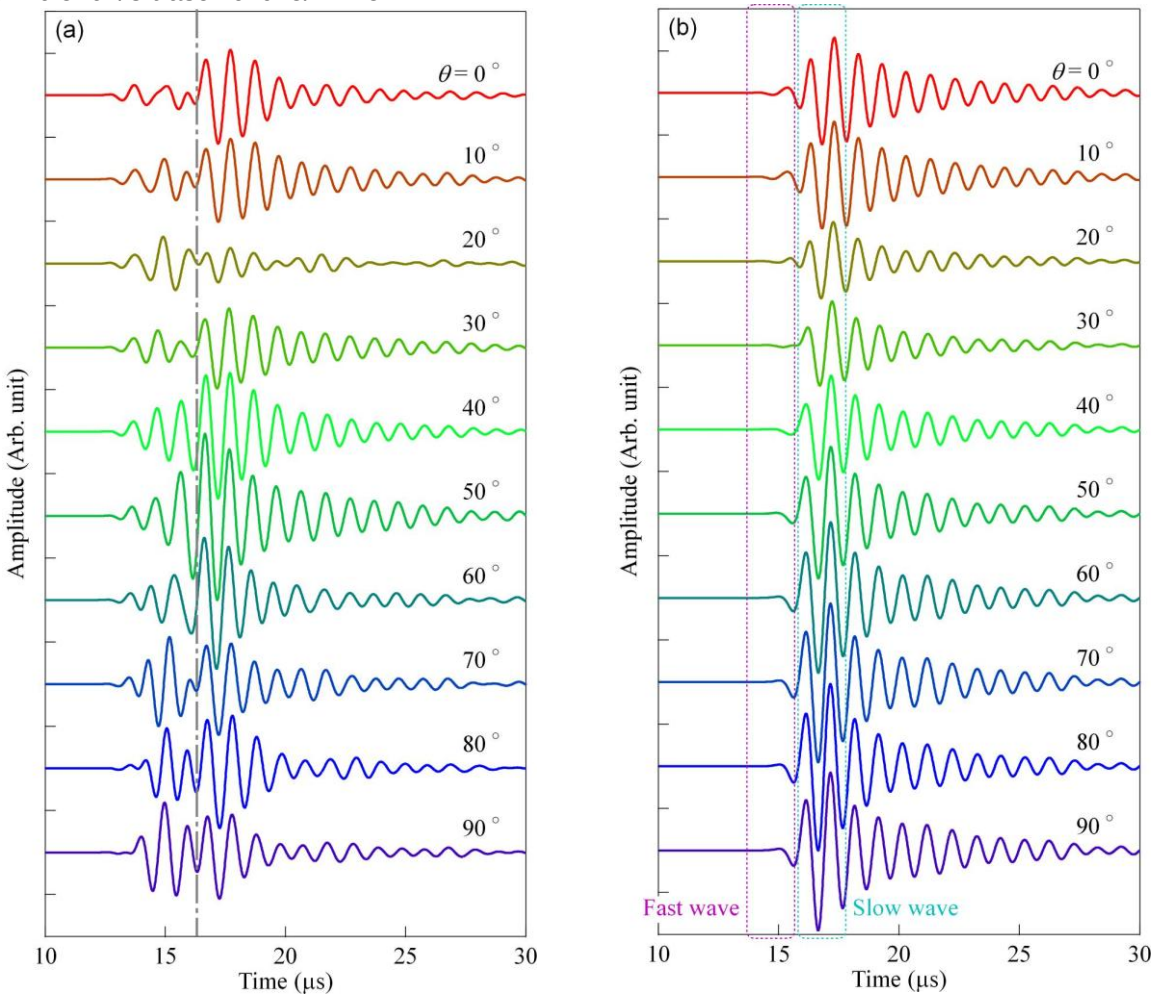

Fig. 4: Calculated waveforms for cancellous bones with a porosity of 0.83 and angles θ = 0–90 ° of the major trabecular orientation in piezoelectric finite-difference time-domain (PE-FDTD) simulations; (a) shows the piezoelectric signals generated in the bones, and (b) shows the ultrasound signals propagated through the bones.

References

[1] E. Fukada and I. Yasuda, Journal of the Physical Society of Japan, vol. 12, pp. 1158–1162, 1957, 10.1143/JPSJ.12.1158.

[2] A. M. Parfitt, Journal of Cellular Biochemistry, vol. 55, pp. 273–286, 1994, 10.1002/jcb.240550303.

[3] L. R. Duarte, Archives of Orthopaedic and Trauma Surgery, vol. 101, pp. 153–159, 1983, 10.1007/BF00436764.

[4] A. Hosokawa and T. Otani, The Journal of the Acoustical Society of America, vol. 103, pp. 2718–2722, 1998, 10.1121/1.418118.

[5] A. Hosokawa, Japanese Journal of Applied Physics, vol. 55, 07KF03, 2016, 10.7567/JJAP.55.07KF03.

[6] S. B. Lang, IEEE Transactions on Biomedical Engineering, vol. 17, pp. 101–105, 1970, 10.1109/TBME.1970.4502706.

[7] J. L. Williams and W. J. H. Johnson, Journal of Biomechanics, vol. 22, pp. 673–682, 1989, 10.1016/0021-9290(89)90017-1.

[8] E. Fukada and I. Yasuda, Japanese Journal of Applied Physics, vol. 3, pp. 117–121, 1964, 10.1143/JJAP.3.117.

[9] S. Saha and P. A. Williams, IEEE Transactions on Biomedical Engineering, vol. 39, pp. 1298–1304, 1992, 10.1109/10.184706.

[10] P. A. Williams and S. Saha, Annals of Biomedical Engineering, vol. 24, pp. 222–233, 1996, 10.1007/BF02667351.

[11] A. Hosokawa and T. Otani, The Journal of the Acoustical Society of America, vol. 101, pp. 558–562, 1997, 10.1121/1.418118.

[12] A. Hosokawa, T. Otani, T. Suzaki, Y. Kubo, and S. Takai, Japanese Journal of Applied Physics, vol. 36, pp. 3233–3237, 1997, 10.1143/JJAP.36.3233.